CHEMISTRY OF MATERIALS
Article

Chem. Mater. **2009,** *21,* 2895–2903 2895
DOI:10.1021/cm900698p

Colloidal Crystal Templating to Produce Hierarchically Porous $LiFePO_4$ Electrode Materials for High Power Lithium Ion Batteries

Cara M. Doherty,[†,‡] Rachel A. Caruso,*[,‡,⊥] Bernd M. Smarsly,[§] and Calum J. Drummond*[,†,⊥]

[†]*CSIRO Molecular and Health Technologies, Private Bag 10, Clayton, Victoria 3169, Australia,* [‡]*School of Chemistry, The University of Melbourne, Victoria 3010, Australia,* [§]*Institute of Physical Chemistry, University of Giessen, Heinrich-Buff-Ring 58, D-35392 Giessen, Germany, and* [⊥]*CSIRO Materials Science and Engineering, Private Bag 33, Clayton, Victoria 3169, Australia*

Received March 12, 2009. Revised Manuscript Received April 25, 2009

Porous $LiFePO_4$ has been prepared via a solution-based templating technique. Beads of poly (methyl methacrylate) were synthesized with diameters of 100, 140, and 270 nm and used to form colloidal crystal templates to produce $LiFePO_4$, which featured pores spanning from 10 to 100 nm. The use of colloidal crystal templates allowed an examination of the effects of pore size on the electrochemical properties. The templated $LiFePO_4$ samples were fully characterized using SEM, TEM, XRD, Rietveld analysis, and nitrogen sorption prior to electrochemical testing. The materials with the largest pores, around 100 nm diameter, gave the best discharge capacities, with 160 mA h g^{-1} at 0.1*C* and 115 mA h g^{-1} at 5*C* being achieved. This compares with a theoretical discharge capacity of 170 mA h g^{-1}.

Introduction

Lithium ion batteries have fast become the dominant rechargeable portable battery since their commercial introduction in the early 1990s. They are renowned for their high energy density; however, future developments will require improving the overall performance, particularly the power capability. Lithium iron phosphate, $LiFePO_4$, is a promising cathode material because of its excellent electrochemical properties (with a theoretical capacity of 170 mA h g^{-1}), low cost, and low toxicity.[1] The major drawback for $LiFePO_4$ is its poor conductivity[1,2] which may be overcome through the addition of conductive carbon[3−8] and incorporating nanostructured designs[9−14] to improve the electrochemical performance.

Increasing the interface between the electrode and the electrolyte, and decreasing the diffusion distance in which the lithium ions must travel, are key properties for optimization when synthesizing high-power electrode materials.[11,14] Porous electrode materials offer the potential to improve the electrochemical properties; however, the optimal pore size and particle morphology has not yet been systematically investigated for $LiFePO_4$. In this paper, the preparation of porous $LiFePO_4$ via a solution-based templating technique is described, using poly(methyl methacrylate) (PMMA) colloidal crystals as templates to produce electrode materials with a range of pore sizes.

In 1997, Velev first reported the use of colloidal latex spheres, in the range of 150 nm to 1 μm as templates to produce silica macroporous structures.[15] Since then, many other inorganic materials such as porous metals, metal oxides, metal carbonates, and polymers have been templated from latex spheres that had been arranged into cubic arrays coined as "colloidal crystals".[16−21] Colloidal

*Corresponding author. E-mail: Calum.Drummond@csiro.au (C.J.D.); rcaruso@unimelb.edu.au (R.A.C.). Tel: 61 3 9545 2057 (C.J.D.); +61 3 8344 7146 (R.A.C.). Fax: 61 3 9545 2059 (C.J.D.); +61 3 9347 5180 (R.A.C.).

(1) Padhi, A. K.; Nanjundaswamy, K. S.; Goodenough, J. B. *J. Electrochem. Soc.* **1997**, *144*, 1188–1194.
(2) Croce, F.; D'; Epifanio, A.; Hassoun, J.; Deptula, A.; Olczac, T.; Scrosati, B. *Electrochem. Solid-State Lett.* **2002**, *5*, A47–A50.
(3) Huang, H.; Yin, S. C.; Nazar, L. F. *Electrochem. Solid-State Lett.* **2001**, *4*, A170–A172.
(4) Prosini, P. P.; Zane, D.; Pasquali, M. *Electrochim. Acta* **2001**, *46*, 3517–3523.
(5) Dominko, R.; Bele, M.; Gaberscek, M.; Remskar, M.; Hanzel, D.; Pejovnik, S.; Jamnik, J. *J. Electrochem. Soc.* **2005**, *152*, A607–A610.
(6) Shin, H. C.; Cho, W. I.; Jang, H. *Electrochim. Acta* **2006**, *52*, 1472–1476.
(7) Fey, G. T. K.; Lu, T. L. *J. Power Sources* **2008**, *178*, 807–814.
(8) Bhuvaneswari, M. S.; Bramnik, N. N.; Ensling, D.; Ehrenberg, H.; Jaegermann, W. *J. Power Sources* **2008**, *180*, 553–560.
(9) Sadoway, D. R.; Mayes, A. M. *MRS Bull.* **2002**, *27*, 590–592.
(10) Sides, C. R.; Li, N. C.; Patrissi, C. J.; Scrosati, B.; Martin, C. R. *MRS Bull.* **2002**, *27*, 604–607.
(11) Attard, G. S.; Elliott, J. M.; Bartlett, P. N.; Whitehead, A.; Owen, J. R. *Macromol. Symp.* **2000**, *156*, 179–186.
(12) Choi, D.; Kumta, P. N. *J. Power Sources* **2007**, *163*, 1064–1069.
(13) Delacourt, C.; Poizot, P.; Levasseur, S.; Masquelier, C. *Electrochem. Solid-State Lett.* **2006**, *9*, A352–A355.
(14) Gibot, P.; Casas-Cabanas, M.; Laffont, L.; Levasseur, S.; Carlach, P.; Hamelet, S.; Tarascon, J. M.; Masquelier, C. *Nat. Mater.* **2008**, *7*, 741–747.
(15) Velev, O. D.; Jede, T. A.; Lobo, R. F.; Lenhoff, A. M. *Nature* **1997**, *389*, 447–448.
(16) Holland, B. T.; Blanford, C. F.; Do, T.; Stein, A. *Chem. Mater.* **1999**, *11*, 795–805.
(17) Antonietti, M.; Berton, B.; Goltner, C.; Hentze, H. P. *Adv. Mater.* **1998**, *10*, 154–159.
(18) Wang, T. W.; Sel, O.; Djerdj, I.; Smarsly, B. *Colloid Polym. Sci.* **2006**, *285*, 1–9.
(19) Sadakane, M.; Takahashi, C.; Kato, N.; Ogihara, H.; Nodasaka, Y.; Doi, Y.; Hinatsu, Y.; Ueda, W. *Bull. Chem. Soc. Jpn.* **2007**, *80*, 677–685.
(20) Sadakane, M.; Horiuchi, T.; Kato, N.; Takahashi, C.; Ueda, W. *Chem. Mater.* **2007**, *19*, 5779–5785.
(21) Stein, A.; Li, F.; Denny, N. R. *Chem. Mater.* **2008**, *20*, 649–666.

Published on Web 06/02/2009

crystals are formed from close-packed spheres, such as poly(styrene) (PS), silica, or PMMA beads that can range in diameter depending on the synthesis conditions. When used as templates, the size of the sphere correlates to the void or pore size in the final structure.[15,21] The first report of forming electrode materials using colloidal crystal templates for use in lithium ion batteries was in 2002.[22] Sakatomo et al. reported the synthesis of V_2O_5 with pores between 10 and 30 nm that delivered higher capacities at higher discharge rates because of improved charge transport.[22] Since then, many other electrode materials have been prepared and tested including SnO_2 anodes, $LiNiO_2$,[23] TiO_2,[24] $Li_4Ti_5O_{12}$,[25] $LiMn_2O_4$,[26] and porous carbon prepared from silica colloids for use in capacitors.[27] Several excellent reviews on electrode materials templated with colloidal crystals for use in lithium-ion batteries are available for a thorough overview of the development of electrode materials.[21,28,29] In this study, PMMA colloidal crystals were used as templates to form porous $LiFePO_4$ electrode materials, enabling the pore sizes to be specifically tailored to allow an investigation into the effects of morphological changes on the electrochemistry.

The PMMA colloidal crystals provided a firm scaffolding onto which the $LiFePO_4$ precursor solution condensed; once removed during calcination, the electrode materials featured pores in the mesopore (2−50 nm), meso-/macropore (20−80 nm), and macropore (50−120 nm) size range depending on the diameter of the initial PMMA template. The aims of this study were to synthesize a range of templates, which would ensure that highly crystalline $LiFePO_4$ materials were formed while maintaining high surface areas, and to compare the electrochemical properties of $LiFePO_4$ samples of varied pore size. The $LiFePO_4$ materials templated with each of the colloidal crystals (polymer bead diameter of 100, 140, and 270 nm), were also calcined at increasing temperatures to investigate the effects of crystallite growth on the morphology and consequently the electrochemistry.

The $LiFePO_4$ templated samples were imaged using microscopy techniques including scanning electron microscopy (SEM) and transmission electron microscopy (TEM). The pore sizes and surface areas of the materials were determined using nitrogen sorption. Sample purity was confirmed with X-ray diffraction (XRD) and Rietveld analysis was used to measure the crystallite size. The samples were then prepared into electrode films and assembled into coin cells in order to galvanostatically test the materials at different rates to investigate how the structure of porous $LiFePO_4$ influences the electrochemical performance.

Table 1. Synthetic Parameters Used to Prepare Colloidal Crystals with Various Diameters

mass of SDS (mg)	mass of KPS (g)	volume of water (mL)	volume of MMA (mL)	SEM particle diameter (nm)
50.0	0.1169	175	15	100−110
12.0	0.1169	175	15	135−145
0.50	0.0292	175	15	265−275

Experimental Section

Preparation of PMMA Colloidal Crystal Template. The PMMA latex spheres were synthesized through emulsion polymerization of methyl methacrylate (MMA) (CH_2=$C(CH_3)COOCH_3$, Aldrich) based on a technique described in the literature.[18,30] The benefit of using PMMA latex colloidal crystals as a template is that the size of the spheres can be easily tailored through the addition of a surfactant during polymerization, which allows fine control over the template structure and consequently the final pore structure in the templated material. PMMA was advantageous as the colloidal crystal template as the wettability of the PMMA with polar solvents such as water was more favorable than that of PS colloids and the template removal with PMMA was much milder than the chemical etching required with silica templates.[18,31] The MMA contained phenolic inhibitors that were removed by filtration through aluminum oxide (Al_2O_3, Sigma-Aldrich). The MMA was then distilled prior to polymerization in Milli-Q water in the presence of sodium dodecyl sulfate (SDS), ($CH_3(CH_2)_{10}-CH_2OSO_3Na$, BDH) as the surfactant and potassium peroxodisulfate (KPS), ($K_2S_2O_8$, BDH) as the initiator. The polymerization occurred at 70 °C under nitrogen for 4 h. Three different-sized templates were prepared by adjusting the amount of SDS during polymerization. The synthesis conditions for the preparations of the three templates are summarized in Table 1.

The PMMA solution began to turn opaque as it started to polymerize and finally formed a milky white colloidal solution. The colloidal crystal solution was poured into a Petri dish and dried under ambient conditions to evaporate slowly overnight. The gradual drying process allowed the spheres to stack up in a close-packed hexagonal array, which was evident by the opal-like reflection from the dried template due to optical diffraction.

Preparation of Porous $LiFePO_4$ using Colloidal Crystal Templates. Mesoporous and macroporous $LiFePO_4$ was formed using the PMMA latex colloidal crystals as templates with bead diameters of 100, 140, and 270 nm. $LiFePO_4$ samples were prepared via water based solution chemistry. Each sample was made with stoichiometric amounts of iron nitrate nonahydrate ($Fe(NO_3)_3 \cdot 9H_2O$, Aldrich), lithium acetate (CH_3COOLi, Aldrich), and phosphoric acid (H_3PO_4, 85 wt %, Sigma-Aldrich). In a typical synthesis, 2.61 g of iron nitrate was first dissolved into 1.0 g of Milli-Q water; 0.42 g of lithium acetate and 0.73 g of phosphoric acid were then added, and the solution was stirred for 2 h to ensure homogeneity. The precursor solution was prepared with a minimal amount of water so that excess solvent

(22) Sakamoto, J. S.; Dunn, B. *J. Mater. Chem.* **2002**, *12*, 2859–2861.
(23) Yan, H. W.; Sokolov, S.; Lytle, J. C.; Stein, A.; Zhang, F.; Smyrl, W. H. *J. Electrochem. Soc.* **2003**, *150*, A1102–A1107.
(24) Bing, Z.; Yuan, Y.; Wang, Y.; Fu, Z. W. *Electrochem. Solid-State Lett.* **2006**, *9*, A101–A104.
(25) Woo, S. W.; Dokko, K.; Kanamura, K. *Electrochim. Acta* **2007**, *53*, 79–82.
(26) Tonti, D.; Torralvo, M. J.; Enciso, E.; Sobrados, I.; Sanz, J. *Chem. Mater.* **2008**, *20*, 4783–4790.
(27) Tabata, S.; Isshiki, Y.; Watanabe, M. *J. Electrochem. Soc.* **2008**, *155*, K42–K49.
(28) Bruce, P. G.; Scrosati, B.; Tarascon, J. M. *Angew. Chem., Int. Ed.* **2008**, *47*, 2930–2946.
(29) Wang, Y.; Cao, G. Z. *Adv. Mater.* **2008**, *20*, 2251–2269.
(30) Zou, D.; Ma, S.; Guan, R.; Park, M.; Sun, L.; Aklonis, J. J.; Salovey, R. *J. Polym. Sci., Part A: Polym. Chem.* **1992**, *30*, 137–144.
(31) Yan, H.; Blanford, C. F.; Lytle, J. C.; Carter, C. B.; Smyrl, W. H.; Stein, A. *Chem. Mater.* **2001**, *13*, 4314–4321.

would not destroy the PMMA template structure. The transparent yellow $LiFePO_4$ precursor solution was added dropwise over a dish containing 4.0 g of dried colloidal crystals. The precursor solution wet the entire template until it was slightly moist to ensure that there was no excess $LiFePO_4$. The samples were then left to dry under airflow overnight prior to calcination. The samples were heated at 2 °C min^{-1} to 220 °C and held at this temperature for 3 h to further condense the inorganic precursor, before heating at the same rate to the desired temperature and remaining at this temperature for a further 3 h. The $LiFePO_4$ samples templated with the three colloidal crystal templates (bead diameters of 100, 140, or 270 nm) were sintered at maximum temperatures of 320, 500, 600, 700, and 800 °C. The samples were calcined under a reducing atmosphere (95% argon and 5% hydrogen) to ensure that Fe(III) was completely reduced to the Fe(II) species. The samples were left under the reducing atmosphere until they had cooled to room temperature.

Characterization. Powder X-ray diffraction (XRD) was used to determine the purity and crystallinity of the samples. Data sets for phase identification were collected using a Philips X'Pert Pro diffractometer with a PW3830/40 generator and Cu Kα radiation. Data was collected from 5 to 70° 2θ, at a step size of 0.02° for 0.45 s per step. Diffraction peaks were labeled and phases identified using XPLOT for Windows, (v. 1.34), the PANalytical software, X'Pert HighScore Plus (v. 2.21(2.2.1)), and the International Centre for Diffraction Data Database Sets 1−57. Data sets used for the determination of crystal size were collected using Co Kα radiation. Data was collected from 5 to 110° 2θ, at a step size of 0.02° for 2.0 s per step. Crystallite sizes and phase abundances were calculated using the Bruker AXS software TOPAS (v. 3) and crystal structures from the ICSD Database, FindIt (v. 1.4.2).

The surface area and pore size distribution of the samples were determined via nitrogen sorption with the Micromeritics Tristar surface area and porosity analyzer, equipped with a 6 port degassing station (Micromeritics VacPrep 061). The samples were degassed under vacuum (≤100 mTorr) at 150 °C for 16 h prior to analysis. The surface area was calculated using the Brunauer−Emmet−Teller (BET) method, and the Barrett−Joyner−Halenda (BJH) pore size distribution was determined using the desorption branch of the isotherm using the Tristar 3000 software package.

The samples were analyzed using a field-emission scanning electron microscope at 5 kV for the $LiFePO_4$ samples and 2 kV for the polymeric colloidal crystals. The samples were coated with iridium prior to analysis to form a conductive layer and prevent charging during analysis. Several samples were analyzed at the Australian Nuclear Science and Technology Organisation (ANSTO) using a JEOL 2012F transmission electron microscope fitted with an EmiSpec E Vision energy-dispersive X-ray (EDX) analysis system.

The carbon content for each of the samples was accurately determined using a Carlo Erba Elemental Analyzer EA 1108 from The Campbell Microanalytical Laboratory, Department of Chemistry, University of Otago, Dunedin, New Zealand.

Electrochemical Analysis. The $LiFePO_4$ electrode films were prepared with 75% active material, 15% Shawinigan carbon black, 10% Kuruha polyvinylidene fluoride (PVDF) binder, and *N*-methyl-2-pyrrolidinon anhydrous (NMP, Sigma-Aldrich) solvent. The synthesized $LiFePO_4$ powder was ground using a mortar and pestle and weighed into a small beaker. The carbon black was added to the $LiFePO_4$ sample, covered, and dry-mixed for 4 h to achieve intimate contact between the $LiFePO_4$ particles and the conductive carbon. The PVDF was then weighed in with enough NMP to obtain a smooth consistency. The slurry was mixed for 16 h before being spread into a film. The aluminum current collector was lightly abraded and cleaned with ethanol prior to coating using a stainless steel guiding roller and achieved loading of approximately 1 mg cm^{-2} (∼50 μm dry film). The films were prepared at the same thickness for valid comparison. The wet film was dried and placed in a vacuum oven at 120 °C overnight. The electrodes were tested in a CR2032 coin cell with 1 M lithium hexafluorophosphate electrolyte ($LiPF_6$, Hohsen) in ethylene carbonate: diethyl carbonate (EC:DEC) 1:1 (v/v), a Teflon Celgard separator (#2400, 16 mm diameter) and lithium ribbon (Sigma-Aldrich). The electrolyte was quickly absorbed by the $LiFePO_4$ electrode film. Capillary action is likely to pull the electrolyte into the mesopores. The electrolyte may not be able to access the micropores which would reduce the capacity of the electrode.

Electrochemical testing was undertaken using a Solartron 1470E multichannel Cell Test potentiostat. Each of the coin cells were galvanostatically charged at 0.2*C* and discharged at different *C* rates of 0.1*C*, 0.2*C*, 1*C*, 2*C*, 5*C* in order to establish the overall performance of the materials at slow and fast rates. The currents used were calculated on the active material only, and the mass of the carbon contribution from the synthesized samples was subtracted so as to keep the results consistent. Impedance measurements were carried out after the cell had been galvanostatically cycled 18 times to ensure that the solid electrolyte interface layer on the cathode had been fully developed and stabilized. The impedance was determined when the cells were in the full state of discharge, using an amplitude AC signal of 5 mV and frequency in the range of 100 kHz − 0.01 Hz.

Results and Discussion

SEM images of the colloidal crystals of each of the three sphere sizes are shown in Figure 1a−c. The images show closely packed, ordered three-dimensional structures. The diameters of the colloids were homogeneous for each of the templates. This promoted well-organized stacking over the long range and provided a good scaffold into which the $LiFePO_4$ precursors could infiltrate. The sphere size was controlled by adjusting the surfactant and initiator concentration (Table 1). Increasing the concentration of SDS in the solution prior to polymerization promoted the nucleation of more micelles and hence reduced the diameter of the PMMA beads. The 100 nm template beads resulted from the addition of 50 mg of SDS, whereas decreasing the amount of SDS (0.50 mg) and initiator increased the final PMMA bead diameters to 270 nm.

The SEM images in Figure 1d−f show the open porous structures of the $LiFePO_4$ templated using the colloidal crystals with the different-sized beads. The samples were calcined at 500 °C and displayed a continuous open lattice structure with long-range order. The calcination process allowed sufficient removal of the PMMA template without destroying the lattice structure. The templated $LiFePO_4$ materials replicate the bulk size and morphology of the colloidal crystal templates and feature rectangular particles that are up to hundreds of micrometers in size (see the Supporting Information, Figure S1).

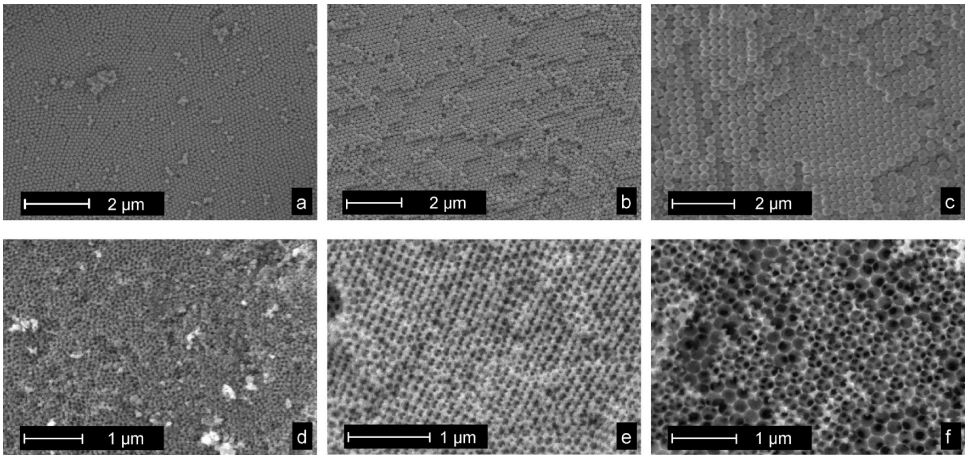

Figure 1. SEM images of the colloidal crystal templates (top) and associated $LiFePO_4$ templated samples calcined at 500 °C (bottom) formed using PMMA beads of diameter (a, d) 100, (b, e) 140, and (c, f) 270 nm, respectively.

Table 2. Bead Diameter for the Colloidal Crystal Template and Resulting Pore Diameters for the Templated $LiFePO_4$ Material Calcined at 500 °C as Determined from SEM Images and N_2 Sorption BJH Pore Analysis

PMMA bead diameter (nm)	SEM pore diameter (nm)	BJH pore distribution (nm)	SEM wall thickness (nm)
100	35−45	10−60	40−60
140	60−70	20−80	50−80
270	90−100	50−120	60−100

The pore sizes for each of the three templated $LiFePO_4$ samples are included in Table 2. The average pore sizes have been determined from SEM image analysis and confirmed with nitrogen sorption data. In general, classical nitrogen physisorption does not allow for the characterization of materials with pore sizes larger than approximately 40 nm, decreasing the accuracy of such values. Nevertheless, applying the BJH approach provides a formal pore size distribution and a formal average pore diameter, giving a reasonable estimate for the pore size and the necks connecting the pores. If the pore size distribution is taken from the desorption branch of the nitrogen sorption data, the calculated pore size corresponds to an average between the pore size and the size of the necks connecting the pores. We are aware that the values obtained can be regarded only as an estimate and are backed up with SEM observations (Table 2).

Shrinkage of the $LiFePO_4$ porous structure was evident for all three samples. The pore diameters for each of the samples were approximately 40% of the initial bead diameter due to shrinkage during the condensation and crystallization processes. The samples underwent condensation as they were slowly heated; removing any residual moisture and organic volatiles and hence condensing the $LiFePO_4$ framework. As the samples crystallized at the higher calcination temperatures, the template further decomposed and the structural forces from crystal growth reduced the pore size of the $LiFePO_4$ lattice. The $LiFePO_4$ samples prepared with the smaller 100 nm PMMA spheres formed pores in the large mesopore size range, whereas the 140 nm spheres produced pores in the meso- to macropore size range and the large 270 nm spheres formed macropores with an average diameter of 100 nm. The wall thickness (or the thickness of the $LiFePO_4$ material between the pores) also increased as the size of the colloidal crystal templates was increased (Table 2). The wall thicknesses varied slightly between samples and were determined using multiple SEM images for each template size and calcination temperature. The images in Figure 1 were of $LiFePO_4$ samples calcined at 500 °C and had thinner walls than those samples calcined at 800 °C.

The open porous lattice was consistent throughout the 140 and 270 nm templated $LiFePO_4$ samples; however, the SEM results found evidence that there were areas within the 100 nm templated samples where the small pores may have collapsed and become blocked during calcination. Several SEM images revealed sections of 100 nm templated $LiFePO_4$ where the open lattice was not present (see the Supporting Information, Figure S2). Some pores were still apparent, evidence that the PMMA colloidal crystals were initially present. Nonetheless, it appears that the condensation and crystallization processes caused parts of the lattice structure to be destroyed. This indicates that if the colloidal crystal diameters were to be further reduced, the porous structures are unlikely to withstand the crystallization process and would not produce a material with mesopores nor high surface areas. The wall thickness of the $LiFePO_4$ templated with 100 nm beads was determined to lie between 50 and 60 nm, which was close to the average crystallite size determined using Rietveld analysis (Table 3); therefore, crystal growth to 80 nm with increased calcination temperatures would cause some structural collapse.

Effects of Calcination Temperature. Each of the three templated materials were calcined at a range of temperatures (320, 500, 600, 700, and 800 °C) in order to investigate the crystallization behavior on both the $LiFePO_4$ morphology and electrochemical properties. The heating rates were kept relatively slow, at 2 °C min^{-1}, to avoid structural collapse from fast crystallization. Thermal gravimetric analysis results indicated that the PMMA template did not start to decompose until temperatures reached 250 °C; therefore, at 220 °C, the template was able to provide some structural support while the

Table 3. Crystallite Diameter, Surface Area, and Carbon Content for $LiFePO_4$ Samples Prepared with the Three Different Template Sizes and Various Calcination Temperatures

	crystallite size for each template size (nm)			BET surface area for templated $LiFePO_4$ ($m^2\ g^{-1}$)			carbon remaining in templated $LiFePO_4$ (%)		
	template diameter (nm)								
calcination temperature (°C)	100	140	270	100	140	270	100	140	270
500	52	43	50	73	58	47	10.2	8.3	7.5
600	57	53	54	67	56	46	10.3	8.1	7.6
700	75	57	66	51	51	45	10.6	8.5	7.1
800	80	74	71	53	42	47	7.2	7.6	6.3

$LiFePO_4$ condensed. The XRD results for the 140 nm templated samples are included in Figure 2 for all calcination temperatures. It is evident from the XRD results that the samples remained amorphous at 320 °C and only crystallized into the olivine triphylite structure at 500 °C and above. All the samples show the pure $LiFePO_4$ phase.

Table 3 highlights the trends between the calcination temperature, surface area and crystallite size for each of the templated samples. The crystallite diameter of the samples consistently grew larger as the annealing temperature increased. The crystallite size grew from approximately 50 to 70 nm when the calcination temperature was increased from 500 to 800 °C.

The porous lattice structures were able to withstand the high calcination temperatures and did not collapse even at 800 °C, indicating that the materials were quite robust. TEM images a and b in Figure 3 show the open porous structure of the $LiFePO_4$ templated particles. The porous lattice structure was evident in samples calcined at both 320 and 600 °C from the 140 nm template. Figure 3b displays the regular channels formed from the close-packed beads, which allow for good electrolyte access to the $LiFePO_4$ surfaces. Structural integrity despite crystal growth was evident in the SEM images of the templated $LiFePO_4$, which were annealed at higher temperatures (Figure 3c).

Nitrogen sorption was used to investigate the effect that calcination temperature and template size together had on the surface area of the $LiFePO_4$. The samples were calcined under a reducing atmosphere to prevent the iron from oxidizing, therefore there was a significant amount of carbon residue left in the sample, which also effects the surface area. Table 3 shows the relationship between surface area and calcination temperature for each of the three template sizes. The results indicate that the smaller the bead diameter in the colloidal crystal, the higher the surface area of the final material. There is a decrease in the surface area for the materials templated with 100 and 140 nm beads with increasing calcination temperature due to the $LiFePO_4$ crystal growth. This was not evident for the sample using the 270 nm beads, because the larger void spaces between the PMMA spheres may have provided for greater accumulation of the $LiFePO_4$, which allowed for crystal growth without substantial change to the structure; therefore, a significant decrease in surface area was not observed. The desorption pore size distribution for the $LiFePO_4$ templated with 270 nm templates (see the Supporting Information, Figure S3) reveals a shift in pore size as the calcination temperature was increased. The prevalence of macropores in the range 50−140 nm decreased, whereas the content of mesopores between 5 and 25 nm increased as the calcination temperature was raised. The shift in pore size distribution explains the relatively constant surface area despite the crystal growth for $LiFePO_4$ samples made with the larger template.

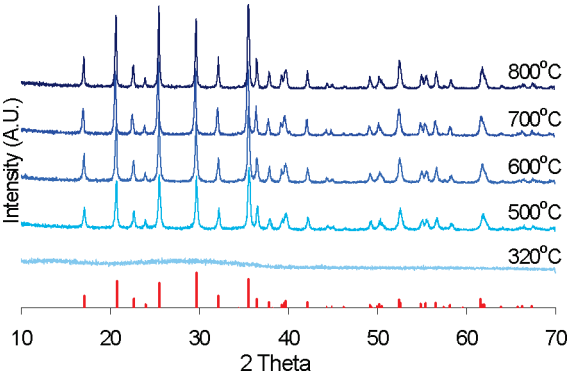

Figure 2. XRD patterns for $LiFePO_4$ templated with colloidal crystals of 140 nm beads calcined at different temperatures. The peaks are indexed to the pure olivine ($LiFePO_4$) phase [40−1499].

The nitrogen sorption isotherms of the samples calcined at 700 °C are displayed in Figure 4a and give an indication of the size and type of pores present in the $LiFePO_4$ templated samples. All isotherms for the different templates feature hysteresis between the desorption and adsorption branches, indicating the presence of mesopores. The isotherm for the smallest bead template shows a type IV isotherm, where the pores are dominated by mesopores (2−50 nm).[32] The isotherm for the largest bead colloidal crystal is relatively flat and has a broad hysteresis, which indicates that macropores are present in the samples. The BJH pore size distributions for these samples, shown in Figure 4b, reveal the large presence of mesopores for the 140 nm template and a much smaller contribution for the 100 nm templated samples. This confirms that the pores from the smaller template may have partially collapsed because of crystal growth, thus reducing the pore volume, and that the surface area is primarily a consequence of the micropores.

Electrochemical Analysis. The templated $LiFePO_4$ samples were prepared as electrodes and assembled into coin cells with a lithium metal anode. The cells were cycled

(32) Sing, K. S. W.; Everett, D. H.; Haul, R. A. W.; Moscou, L.; Pierotti, R. A.; Rouquerol, J.; Siemieniewska, T. *Pure Appl. Chem.* **1985**, *57*, 603–619.

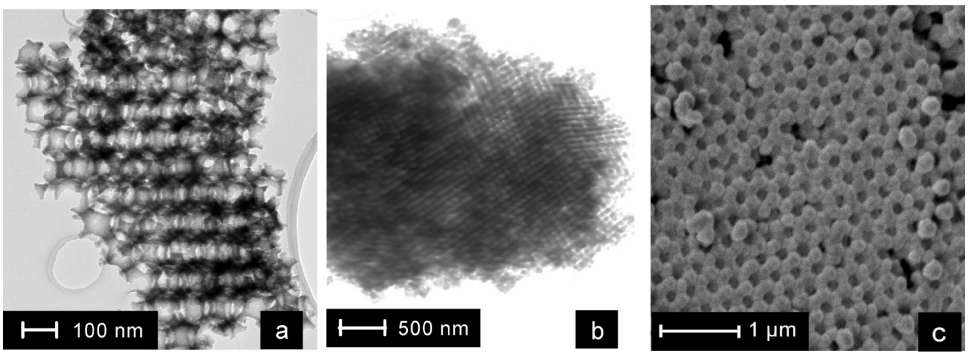

Figure 3. (a) TEM image of 140 nm bead-templated $LiFePO_4$ calcined at 320 °C and (b) calcined at 600 °C. (c) SEM image of 270 nm bead-templated $LiFePO_4$ calcined at 700 °C showing the ability of the lattice structure to withstand both the crystallization process and particle growth.

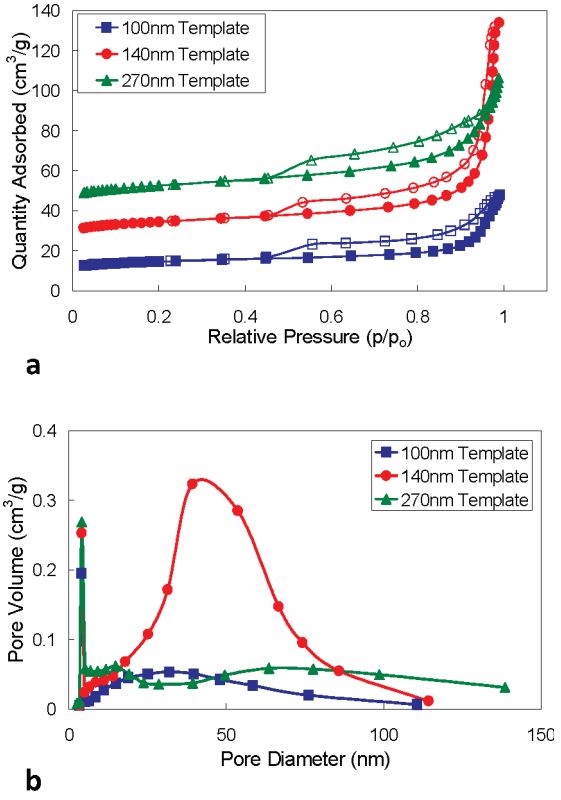

Figure 4. Nitrogen sorption results for $LiFePO_4$ samples calcined at 700 °C. (a) N_2 isotherms; filled markers denote the adsorption branch and open markers the desorption branch of the isotherm. The 140 and 270 nm isotherms have been offset by 20 and 40 $cm^3\ g^{-1}$, respectively, for clarity. (b) BJH desorption pore size distribution.

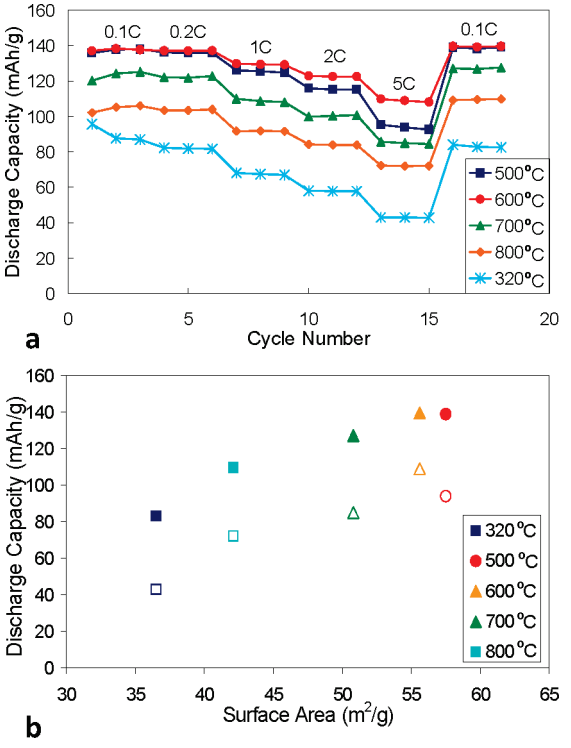

Figure 5. (a) Discharge capacities for $LiFePO_4$ templated with 140 nm colloidal crystals and calcined at different temperatures, and (b) average capacity versus surface area for samples (filled markers discharged at 0.1*C* and open markers at 5*C*).

three times at 0.1, 0.2, 1, 2, and 5*C* discharge rates to determine the available capacity for each sample and finally cycled again at 0.1*C* to ensure that the electrode had completely recovered from the cycling at high *C* rates. The currents used at each *C* rate were calculated from the mass of $LiFePO_4$ in each electrode. The mass of carbon was not included as active electrode material. Figure 5a shows the discharge rates of the $LiFePO_4$ templated with 140 nm colloidal crystals. There is a clear dependence of the capacity of the material on the calcination temperature of the samples. The amorphous sample calcined at 320 °C had significantly poorer discharge capacity with a maximum at 84 mA h g^{-1} at a slow *C* rate of 0.1*C* and only 43 mA h g^{-1} at a high rate (5*C*). This confirmed that the crystallinity of the $LiFePO_4$ had a considerable impact on the performance of the electrode material and that poorly crystalline or amorphous samples were not suitable for high capacity applications. The samples calcined at 600 °C showed the highest capacities of 138 mA h g^{-1} at 0.1*C* and 110 mA h g^{-1} at 5C. The 500 °C sample had equivalent capacities at low discharge rates of 0.1 and 0.2*C*. Notably, the improved crystallinity of the 600 °C calcined sample allowed higher capacities to be achieved at high discharge rates.

There is a correlation between the discharge capacities and the surface areas of the 140 nm templated samples. The templated sample calcined at 320 °C remained amorphous and had a low surface area because of the presence of partially decomposed template (carbon content was as high as 30% for samples calcined at 320 °C, three times as much as samples calcined at 500 °C or above, Table 3). As the calcination temperature increased to 500 °C, the

surface area increased substantially, but as the temperatures further increased, the surface areas decreased because of crystallite growth. Figure 5b indicates that as the surface area of the templated $LiFePO_4$ samples increased, the discharge capacities at both slow and fast discharge rates improved. Increasing the surface area by producing an open porous lattice increases the electrode−electrolyte interface, and therefore improves the capacity of the electrode material. For the 140 nm templated samples, particle morphology and surface area appear to have a significant effect on the electrochemical performance. The capacities achieved are affected considerably by both the morphology and crystallinity of the $LiFePO_4$ electrode. There is consequently a trade-off between attaining high surface areas and the crystallization process.

The $LiFePO_4$ samples templated with the larger 270 nm colloidal crystals, did not show a significant change in the surface area as the calcination temperature was increased (Table 3), therefore the electrochemistry results for the samples templated from the larger spheres reflect the effects from increasing the calcination temperatures, such as the size of the $LiFePO_4$ crystals and the amount of residual carbon. Figure 6a shows the discharge capacities for 270 nm templated $LiFePO_4$ samples calcined between 500 and 800 °C. High discharge capacities of 160 mA h g^{-1} were reached at low discharge rates, which is very close to the theoretical capacity of 170 mA h g^{-1}.[1] It is important to note that at high discharge rates, the samples calcined at higher temperatures 700 and 800 °C have significantly higher capacities (115 mA h g^{-1}) than the samples calcined at lower temperatures. This was likely caused by increased sintering between particles at the higher temperatures as demonstrated by comparing Figure 1f and Figure 3c. Hence the sample calcined at 700 °C should have more intimate contact at the grain boundaries compared to the sample calcined at 500 °C, which would improve the charge transfer between particles.

Figure 6b shows the discharge profiles for the $LiFePO_4$ samples templated with the 270 nm colloidal crystals at different *C* rates. Flat discharge plateaus at 3.4 V are present for both samples at the slow *C* rate of 0.1*C*. The potential of the discharge plateau dropped as the rates were increased, which was a result of polarization within the electrode material. The polarization was caused by slow charge transfer due to resistance from the $LiFePO_4$ electrode.[12,33] The sample calcined at 800 °C had significantly less polarization than the sample calcined at 500 °C (Figure 6b), which indicated that the higher temperature improved the conductivity due to increased sintering.

This trend was confirmed with the AC impedance spectroscopy results (Figure 7). The Nyquist plot revealed the impedance associated with the charge-transfer resistance and diffusion of lithium ions through the bulk of the cathode material.[6] The charge transfer resistance is reflected in the diameter of the semicircle along the real axis.

(33) Mi, C. H.; Zhang, X. G.; Zhao, X. B.; Li, H. L. *J. Alloys Compd.* **2006**, *424*, 327–333.

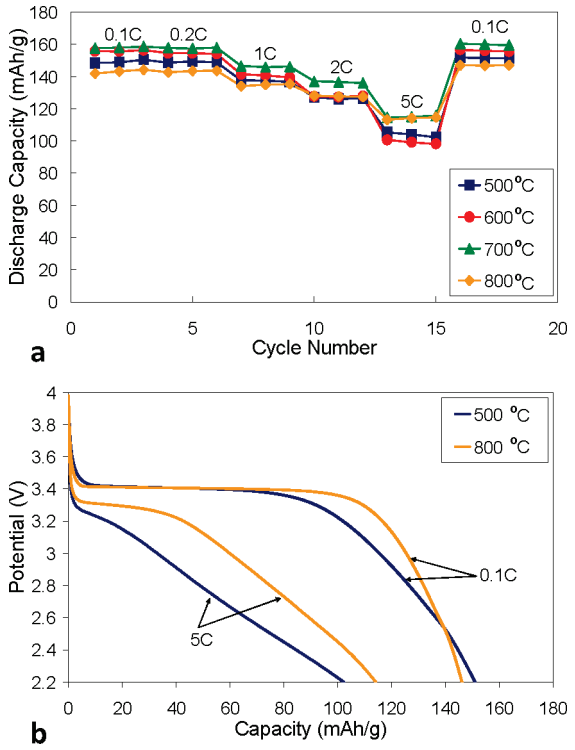

Figure 6. (a) Discharge capacity for $LiFePO_4$ templated with 270 nm beads and calcined at various temperatures, and (b) discharge profiles for samples calcined at 500 and 800 °C at 0.1*C* and 5*C*.

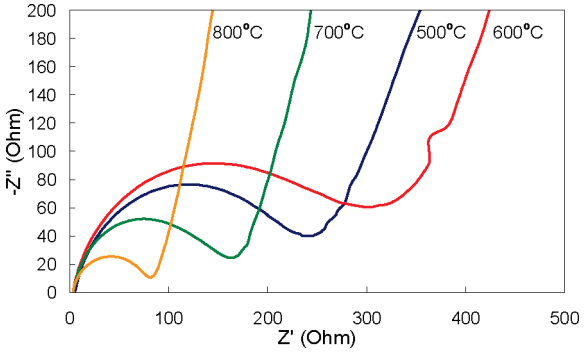

Figure 7. AC impedance spectroscopy for 270 nm colloidal crystal templated $LiFePO_4$ samples calcined at different temperatures.

Figure 7 shows a significant difference between the samples, with the samples calcined at the higher temperatures of 700 and 800 °C having lower charge transfer resistance compared to those calcined at 500 and 600 °C. The charge transfer resistance for the $LiFePO_4$ sample calcined at 800 °C is lower than that of the sample calcined at 700 °C despite having similar surface areas, due to the improved sintering at particle grain boundaries at higher calcination temperatures. These results are consistent with the electrochemical performance of the materials at high discharge rates as demonstrated in Figure 6a. This indicated that the charge transfer between the particles was a significant factor for the high rate performance of the 270 nm colloidal crystal templated $LiFePO_4$ electrodes.

The benefit of using colloidal crystals as templates is that the PMMA bead sizes can be easily tailored in order to change the pore size of the $LiFePO_4$ cathode material. Comparing the discharge capacities of the three different

templated samples shows that the samples prepared with the 270 nm templates have consistently higher discharge capacities than the samples made with smaller diameter templates, across all calcination temperatures (see the Supporting Information, Figures S4 and S5). These results show that although the smaller diameter templates produce the greater surface areas, increasing the electrode−electrolyte interface and decreasing the diffusion distance for the lithium ions, there are other elements influencing the electrochemical properties of the templated materials.

The 270 nm templated samples consistently outperformed the 140 and 100 nm samples (Figure 8a). The morphology of the three different-sized templated samples must be carefully considered with respect to the trends seen. The $LiFePO_4$ samples templated with the 270 nm colloidal crystals feature much larger pores in the range of 10−120 nm. This may allow improved electrolyte access, especially in the case of large $LiFePO_4$ particles, up to hundreds of micrometers in diameter (see the Supporting Information, Figure S1). The micropores such as those seen in the samples templated with the smaller beads may restrict the electrolyte access in such large particles, causing poor interconnectivity between the pores and leaving some $LiFePO_4$ surface electrochemically inactive.

The samples templated with the smallest 100 nm colloidal crystals had the poorest electrochemical performance (Figure 8a). This may have been due to the increased amount of carbon present in the samples (Table 3). The smaller colloidal crystal templates required more PMMA template per mole of $LiFePO_4$, as prepared during synthesis, to ensure that there was no excess precursor solution that would produce nonporous material. This explains why the smaller diameter templates had increased levels of residual carbon in the samples. It is likely that more carbon would be trapped within the large micrometer-sized $LiFePO_4$ particles because of the presence of smaller pores. The addition of carbon to the $LiFePO_4$ samples is a common method for improving the electrodes conductivity and overall electrochemical performance. However, it has been documented that excess carbon can reduce the performance of the electrode material.[5,34] Excess carbon not only degrades the lithium ion diffusion, but blocks the small pores, further preventing the electrolyte from fully infiltrating into the pores at the center of the $LiFePO_4$ particles.

Some pores appeared to collapse during the crystallization process in the 100 nm templated samples. Some regions in the SEM images confirmed degradation of the open lattice (see the Supporting Information, Figure S2). There may be areas of the 100 nm templates samples that have reduced porosity because of structural collapse, and this would explain the poor capacities achieved compared to the samples templated with the 140 nm beads. Further indication that there could have been pore collapse is the

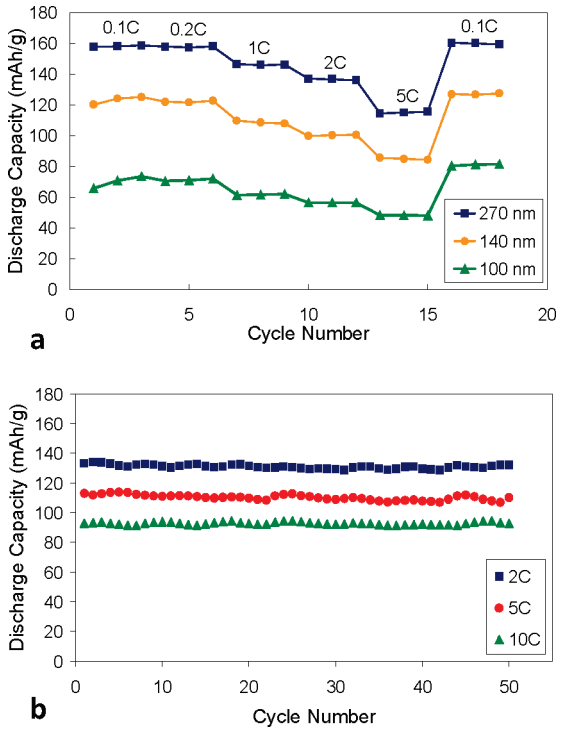

Figure 8. (a) Comparison of discharge capacity for $LiFePO_4$ calcined at 700 °C and templated with different sized colloidal crystal templates and (b) cyclability of $LiFePO_4$ sample templated with 270 nm colloidal crystal and calcined at 700 °C.

significantly lower pore volume, as indicated in Figure 4b, where the 100 nm templated sample had a much smaller pore size distribution peak compared to that of the 140 nm sample, suggestive that the high surface areas were due to micropore contribution, which restricts electrolyte access.

Interconnectivity of the $LiFePO_4$ pore structure is essential for good electrolyte penetration as well as efficient charge transfer. The templated samples prepared with the large 270 nm templates may offer both good interconnectivity and better electrolyte access to surfaces within large micrometer-sized $LiFePO_4$ particles. Lower carbon levels combined with an open porous structure have proved to offer the best electrochemical performance. The sample with the highest capacity was templated with colloidal crystals of beads with 270 nm diameters and calcined at 700 °C. This sample was tested for its long-term performance by cycling the electrodes 50 times at high *C* rates. High discharge rates were used to get a better understanding of the limitations of the coin cell; the coin cells were cycled at 2, 5, and 10*C*. Figure 8b shows the stable discharge capacities of the cells over 50 cycles. Excellent capacities were achieved at high discharge rates. Capacities of 130 mA h g^{-1} were reached at 2*C*, 115 mA h g^{-1} at 5*C*, and 93 mA h g^{-1} was obtained at the 10*C* discharge rate. There was no apparent degradation of the cells after cycling 50 times at these high discharge rates, confirming the stability of the porous electrode materials when templated with 270 nm colloidal crystals.

Although it is difficult to compare the electrochemical results between laboratories because of the different electrode preparation and testing programs used, it is useful to observe progress made among the research

(34) Doeff, M. M.; Hu, Y.; Mclarnon, F.; Kostecki, R. *Electrochem. Solid-State Lett*. **2003**, *6*, A207–A209.

community. Results from solution-based synthesis are very dependent on the synthesis procedures; Gaberscek reported achieving 125 mA h g^{-1} at 1*C* and 75 mA h g^{-1} at 10*C* rates for $LiFePO_4$ particles that were between 1 and 20 μm in diameter and featured 50 nm pores.[35] Lu prepared $LiFePO_4$ using 400 nm PMMA bead templates and had discharge capacities of 145 mA h g^{-1} at 1*C* and 100 mA h g^{-1} at 5.9*C*.[36] Further improvements have recently been achieved with the preparation of nanometer sized $LiFePO_4$. Masquelier's group reported a high capacity of 150 mA h g^{-1} at 2*C*[13] and 147 mA h g^{-1} at 5*C*[14] from nanometer $LiFePO_4$ particles of diameters 100−200 and 40 nm, respectively. The results presented in this paper compare well with previously published solution-based synthesis techniques; however, the results from Masquelier's nanoparticle work appear very promising. Combining the preparation of the nanoparticles with a three-dimensional templated framework, such as that reported here, may allow for good particle interconnectivity and efficient electrolyte access which is the key to optimizing $LiFePO_4$ electrode materials. The advantage of using colloidal crystal templating to produce high power $LiFePO_4$ electrodes is that it increases the surface area and decreases the diffusion distance while maintaining an interconnected porous structure to provide efficient charge transfer and reduced impedance. This technique allows the pore sizes to be tailored while controlling the synthesis conditions, which enables an investigation to be undertaken on the effects of pore sizes and sintering conditions on the electrochemistry.

Conclusion

Lithium iron phosphate was successfully templated using colloidal crystal templates of 100, 140, and 270 nm diameter spheres to produce porous, open lattice electrode materials, which featured pores in the mesoporous (10−50 nm), meso−macroporous (20−80 nm), and macroporous (50−120 nm) ranges, respectively. The well-stacked PMMA colloidal crystals provided robust scaffolding around which the $LiFePO_4$ precursor solution condensed. Once the PMMA spheres were removed through the calcination process, the $LiFePO_4$ featured an open lattice structure with residual carbon left over from the decomposed colloidal crystal template. The three different-sized templated materials were calcined at various temperatures between 320 and 800 °C to investigate the optimal processing conditions in which to obtain high-power energy storage materials.

The electrochemical performance was affected by various properties of the electrode materials, including surface area, morphology, carbon content, and crystallinity. It was found that the macropores produced using the 270 nm colloidal crystal template offered both high surface areas and improved access to the active $LiFePO_4$ material, and hence this sample was able to obtain good discharge capacities of 160 mA h g^{-1}, which was close to the theoretical capacity. The $LiFePO_4$ materials also performed better at high discharge rates with capacities of 115 mA h g^{-1} reached at 5*C*. Higher calcination temperatures were advantageous, as they allowed increased sintering between particles, thus improving charge transfer and reducing electrode polarization.

The $LiFePO_4$ templated samples prepared with the 140 nm colloidal crystal templates showed a correlation between the surface area and discharge capacities as the sample calcination temperature was increased. Good crystallinity was essential for good discharge rates; however, as the calcination temperature increased, the crystallite sizes of the $LiFePO_4$ also increased, producing lower surface areas. These lower surface areas, combined with the possibility of limited pore access to parts of the active material, decreased the performance of the 140 nm templated materials compared to the 270 nm templated samples.

The samples templated with the smallest beads consistently had the poorest performance of the three templated samples. The smaller pores could not withstand the crystallization process and the pore collapse or excessive carbon residue meant that the electrolyte could not get access to the $LiFePO_4$ surfaces to achieve high capacities.

Analysis of the $LiFePO_4$ samples templated with different-sized colloidal crystal spheres revealed that the optimal processing conditions produced crystalline $LiFePO_4$ (calcined at 700 °C). The high surface area materials with macropores in the 50−120 nm range allowed good electrolyte access to the $LiFePO_4$ and enhanced electrochemical properties.

Acknowledgment. C.J.D. is a recipient of an Australian Research Council (ARC) Federation Fellowship. This project was also funded under a CSIRO PhD studentship to C.M.D. Further financial support in terms of a University of Melbourne/CSIRO Collaborative Research Grant Scheme, an Albert Shimmins Writing-up Award, a Postgraduate Overseas Research Experience Scholarship from The University of Melbourne that enabled travel to The Max Planck Institute of Colloids and Interfaces, and an Australian Institute of Nuclear Science and Engineering award (AINGRA07027) for access to research equipment at the Australian Nuclear Science and Technology Organisation are also acknowledged. Dr. San Thang assisted with distillation and polymerization techniques, Mr. Mark Blackford with the TEM measurements, and Dr. Anthony Hollenkamp, Dr. Gregory Wilson, and Arek Liewendewski assisted with preliminary optimization of the electrode and coin cell fabrication.

Supporting Information Available: SEM images of bulk PMMA and $LiFePO_4$ particles; SEM images of 100 nm templated $LiFePO_4$; pore size distribution of 270 nm templated $LiFePO_4$; and discharge capacities for templated $LiFePO_4$ samples calcined at 500, 600, 700, and 800 °C (PDF). This material is available free of charge via the Internet at http://pubs.acs.org.

(35) Gaberscek, M.; Dominko, R.; Bele, M.; Remskar, M.; Jamnik, J. *Solid State Ionics* **2006**, *177*, 3015–3022.
(36) Lu, J. B.; Tang, Z. L.; Zhang, Z. T.; Shen, W. *Mater. Res. Bull.* **2005**, *40*, 2039–2046.